POLITECNICO DI TORINO
Repository ISTITUZIONALE

Experimental modeling and aggregation strategy for thermoelectric refrigeration units as flexible loads

Original
Experimental modeling and aggregation strategy for thermoelectric refrigeration units as flexible loads / Diaz-Londono, C., Enescu, D., Ruiz, F., Mazza, A.. - In: APPLIED ENERGY. - ISSN 0306-2619. - ELETTRONICO. - 272:(2020), p. 115065. [10.1016/j.apenergy.2020.115065]

Availability:
This version is available at: 11583/2832093 since: 2020-06-03T16:28:06Z

Publisher:
Elsevier

Published
DOI:10.1016/j.apenergy.2020.115065

Terms of use:

This article is made available under terms and conditions as specified in the corresponding bibliographic description in the repository

Publisher copyright

(Article begins on next page)

10 October 2026

Experimental Modeling and Aggregation Strategy for Thermoelectric Refrigeration Units as Flexible Loads

Cesar Diaz-Londono[a,b,*], Diana Enescu[c], Fredy Ruiz[b,d], Andrea Mazza[a]

[a] *Dipartimento Energia "Galileo Ferraris", Politecnico di Torino, Torino, Italy.*
[b] *Departamento de Electrónica, Pontificia Universidad Javeriana, Bogotá, Colombia.*
[c] *Electronics Telecommunications and Energy Department, Valahia University of Targoviste, Targoviste, Romania.*
[d] *Dipartimento di Elettronica, Informazione e Bioingegneria, Politecnico di Milano, Milano, Italy.*

Abstract

In the last years, the interest regarding thermoelectric refrigerators has increased thanks to their properties such as the absence of moving parts and toxic or fire-sensitive refrigerants, robustness, and low weight. These devices are also quite flexible and may represent a suitable solution to offer grid services to proper demand response programs. In this article, an aggregation strategy is proposed to fulfil system operator requests on power deviations with limited information exchange between the aggregator and each refrigerator. Downward and upward flexibility in energy consumption can be offered, allowing an aggregated set of loads to provide balancing services such as frequency containment reserve, frequency restoration reserve or replacement reserve to the electrical grid. First, a dynamic model of a thermoelectric refrigerator is built and validated using experimental data collected from a real device under controlled and replicable experimental conditions. A modified temperature controller is proposed and an aggregation strategy with reduced communication requirements is formulated. Then, the aggregation of thermoelectric refrigerators is represented with a linear model to determine that this aggregation can behave as flexible load for reserve provision and demand response applications. It is shown through extensive simulations that a set of refrigerators can operate as in a flexible way by modifying their internal temperature set points, responding in less than 30 seconds to any power deviation command and sustaining the modified consumption for up to 15 minutes in the frequency containment and restoration reserves services, and up to 1 hour in the replacement reserve service, without overshoots, rebounds, or synchronization problems.

Keywords: ThermoElectric Refrigerator, Demand Side Flexibility, Demand Response, Frequency Containment Reserve, Balancing Services, Aggregator.

*Corresponding author
Email addresses: cesar.diazlondono@polito.it (Cesar Diaz-Londono), diana.enescu@valahia.ro (Diana Enescu), fredy.ruiz@polimi.it (Fredy Ruiz), andrea.mazza@polito.it (Andrea Mazza)

Nomenclature

c	Counter
e_r	Error
f	TER flexibility state
j	Experiment number
k	Time slot
n	Number of flexible loads participating in energy services
r	The requested power by the system operator
s	Steady state variable
t	Time
t_{ch}	Informs if the set-point change is reached, $\{0, 1\}$
x	Data
C	Thermal capacitance, $\mathrm{J{\cdot}K^{-1}}$
C_{PID}	PID Controller function used in the TER
E	Percent error, %
FIT	Measure of similarity, %
$Flex$	Flexibility information
$G(s)$	Transfer function
I_p	Peltier electric current, A
J	Number of experiments
K_p	Peltier thermal conductance, $\mathrm{W{\cdot}K^{-1}}$
N	Operation time of the TER
N_s	Number of samples
P	Electric power of the TER, W
P_T	Total electric power, W
$\dot{Q}_c$	Heat flow rate absorbed by the TEC, W
$\dot{Q}_h$	Heat flow rate rejected by the TEC, W
R_p	Peltier electrical resistance, Ω
R	Thermal resistance, $\mathrm{K{\cdot}W^{-1}}$
T	Temperature, K
U	Electrical potential, V
V_α	Seebeck voltage, V
V_{in}	Voltage supplied to the TER, V

Greek symbols

α	Seebeck coefficient, $\mathrm{V{\cdot}K^{-1}}$
β_{sys}	Vector with the temperature set-point state
γ	$C_{PI,AGG}$ output
σ	Standard deviation
ρ	Power ramp-rate, $\mathrm{W{\cdot}s^{-1}}$
τ_c	Cold time constant, s
τ_h	Hot time constant, s
ΔT	Temperature difference, K

Subscripts

amb	ambient
c	cold
d	disturbance
dw	down
h	hot
in	inner
inf	information
max	maximum
min	minimum
nor	normal
out	outer
p	Peltier
ref	reference
sp	set-point
TR	TER
u	up

Abbreviations

AC	**A**lternating **C**urrent
ADC	**A**nalog **D**igital **C**onverter
AGG	**Agg**regator
COP	**C**oefficient **o**f **P**erformance
DC	**D**irect **C**urrent
DR	**D**emand **R**esponse
DSF	**D**emand **S**ide **F**lexibility
DSR	**D**emand **S**ide **R**esponse
ENTSO-E	**E**uropean **N**etwork of **T**ransmission **S**ystem **O**perators for **E**lectricity
FCR	**F**requency **C**ontainment **R**eserve
FRR	**F**requency **R**estoration **R**eserves
FSA	**F**ood **S**tandards **A**gency
FSANZ	**F**ood **S**tandards **A**ustralia **N**ew **Z**ealand
$L\&S$	**L**ogical and **S**equential
MAXAE	**Max**imum **A**bsolute **E**rror
PID	**P**roportional **I**ntegral–**D**erivative
PWM	**P**ulse-**W**idth **M**odulation
RES	**R**enewable **E**nergy **S**ources
RMSE	**R**oot **M**ean **S**quared **E**rror
RR	**R**eplacement **R**eserves
SO	**S**ystem **O**perator
TEC	**T**hermo**e**lectric **C**ooler
TER	**T**hermo**e**lectric **R**efrigerator
UCTE	**U**nion for the **C**oordination of the **T**ransmission of **E**lectricity
VCR	**V**apour **C**ompression **R**efrigeration

1. Introduction

In the last years, the share of generation based on Renewable Energy Sources (RES) increased. For example, in the European Union, the share of RES production in 2016 reached 29.6% [1] and more than 40% of this RES production came from photovoltaic and wind sources [2]. The presence of this large share of non-controllable energy sources introduces new uncertainties in the system operation, mostly linked to the unknown generation patterns, that are dependent on variable weather conditions. This phenomenon is leading to a shift from a "generation following load" to the new "load following generation" paradigm [3], requiring the introduction of Demand Side Response (DSR) programs, in which consumers become directly engaged in the operation of the electrical system, as well as tools for the evaluation and the optimization of the available flexible loads [4]. This larger and larger engagement of the customers in the grid operation is also aligned with the recent European energy rulebook [5], which aims to introduce a "clean and customer-centric" energy system and that led to the approval of eight EU directives.

DSR programs can be direct or indirect. In the first case, the modification of energy consumption is made directly by a third party, e.g., an aggregator or retailer, with the preliminary permission of the customer. Examples of these strategies can be found in [6] and [7]. In the second case, customers are incentivized to modify their consumption through payments or penalties, but the decision to intervene on the loads is let to the user, see e.g., [8] and [9], where different contracts for indirect DSR are proposed. These two concepts have evolved in the literature. In fact, the term DSR relates more with the *consumption variation* carried out directly by customers, whereas Demand Side Flexibility (DSF) focuses on the consumption variation that the load (appliances) can offer to the grid [10]. Considering commercial and residential loads, Figure 1 shows some examples of flexible loads in Demand Response (DR) programs [11].

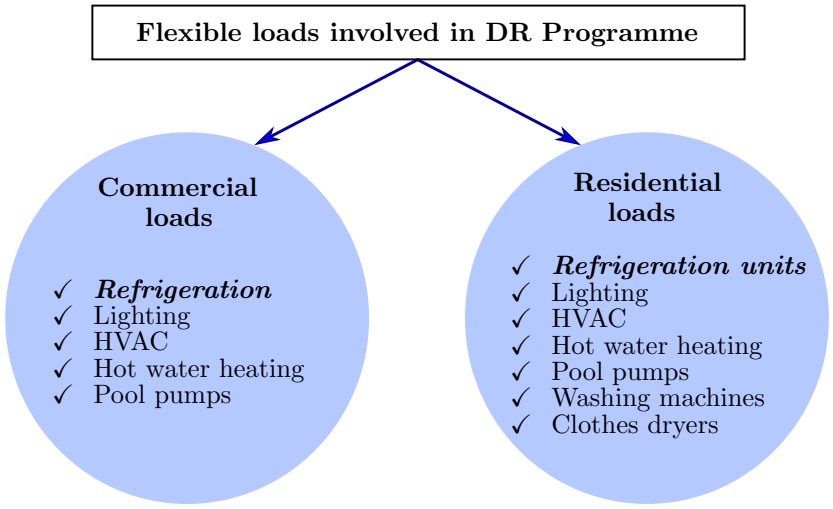

Figure 1: Types of commercial and residential loads involved in the DR program.

The European Smart Grids Task Force, in [12], defines flexibility as "the ability of a cus-

tomer (prosumer) to deviate from its normal electricity consumption (production) profile, in response to price signals or market incentives". This definition highlights the *responsiveness* that the load should guarantee, which also means that the response should respect well-defined shapes, characterized by "ramp-up" and "ramp-down" limits, to properly face the generation variability.

All the previous discussion is based on the *willingness* of the customer to be involved in DSF programs. An overestimation of this aspect can reduce the effectiveness of the program itself [13]. Furthermore, a debate has recently emerged regarding the actual convenience of DSF programs actively involving the customers. For example, in [14] it is shown that even if having more flexibility reduces the overall cost of the system, the load shift from peak to off-peak hours leads to a price variation that can eventually affect the willingness of the customers to be involved in such programs.

For overcoming these issues, a possibility is the larger and larger involvement of loads that can change their consumption *without significantly* affecting the comfort or quality of life of the customers. In this way, customers may be more responsive when called to participate in the program. For instance, Thermostatically Controlled Loads (TCL) such as refrigerators and boilers are suitable to this purpose because, thanks to their thermal inertia, they offer high flexibility in demand consumption. It is worth to note that some types of TCLs, such as air conditioning systems, have been largely studied in literature on demand response. However, their availability for DSF programs is subject to the desired comfort level of the customers (that can vary widely from person to person), as well as on the occupancy level of the spaces, making more challenging and uncertain the use of these systems as flexible loads [15].

In order to evaluate the flexibility in energy consumption of any set of loads and the services that these systems can offer to the power grid, it is required to develop proper dynamic models of the loads behaviour. In the literature on TCLs, two approaches have been followed to derive these models, either by *abstract mathematical* models, which do not aim to represent the physical phenomena that operate the energy conversion, see e.g. [16] and [17], or by *technology-based* models, which aim to characterize in detail the behaviour of the device under analysis.

With regards to the second approach, the flexibility of commercial and residential TCLs is quantified using physical and data-driven models derived from historical data in [18]. Reference [19] proposes a stochastic battery as a model of the aggregated flexibility of a collection of TCLs, departing from a first-principle model of each single system. Vapour compression refrigerators have been experimentally modelled in [20] with the aim to be applied in primary frequency regulation[1]. The model is calibrated and used to show how, by aggregating loads, a "natural" consumption synchronization exists. Reference [22] presents a model of TCLs, based on real measurements of domestic refrigerators. It has been applied to different use case scenarios, to evaluate how different demand response strategies can impact on the aggregated power, ramping rates and overshoot peaks. In [23], the authors present models of electric boilers to be deployed for direct demand response purposes. The models are validated with experimental data and then adopted to predict the power demand when

[1]The UCTE called primary frequency regulation the service that today ENTSO-E calls Frequency Containment Response [21]

used as interruptible loads. All the previous works consider ON-OFF strategies as low-level temperature controllers and one of the challenges that emerges from the analyses is the consumption synchronization, noticed already in [24]. This phenomenon must be handled by the high level controllers that act as aggregators, [25]. In this sense, [19] uses a priority-stack-based control framework to select the TCLs to activate at any time. A Model Predictive Control (MPC) strategy is developed in [26] to optimally schedule TCLs, the energy balance is handled by an optimization problem and a temperature priority list is employed to manage the ON-OFF temperature controllers. In [27], a distributed MPC strategy is proposed to offer regulation services with TCLs, considering lockout times in the switching cycles. In a different way, Reference [28] proposes to intervene in the fan speed controller of HVAC systems to offer flexibility, without using the temperature controller.

This work follows the technology-based approach and presents the development and experimental validation of a model for a ThermoElectric Refrigerator (TER). A TER is a solid-state energy-conversion technology that exploits the Peltier effect to convert electrical energy into thermal energy for heating or cooling [29]. The TER is a very flexible unit that can be included in demand management systems, provided that it is properly installed and its operation occurs within the recommended range of operating temperatures [30]. In previous works the authors have evaluated the energy efficiency and temperature regulation performance of different control strategies for a TER, see [31], where it is shown that a Proportional-Integral–Derivative (PID) controller allows to reduce energy consumption with respect to a ON-OFF controller and also produces a smooth power request to the grid. They have also evaluated the flexibility in the load profile of a TER when the temperature set-point is modified, see [32], where it is shown that by varying the temperature set-point, it is possible to reduce or augment the power demand, achieving a new steady state in less than one hour. To the authors' knowledge, there are no other results about using TERs as flexible loads, neither have been addressed the characteristics of an aggregator for controlling a set of TERs within DSF programs.

This paper proposes an aggregation strategy for TER loads that could provide balancing services to the power grid. First, a detailed model of the energy consumption dynamics of a TER is presented. The model is able to reproduce experimental temperature data with an error lower than 1°C also in transient conditions. Then, based on the evaluation of the power demand response of a set of heterogeneous TERs under temperature set-point changes, a modified PID temperature controller is proposed and it is determined that the TERs can offer balancing services to the grid, responding to power requests within 30 seconds, guaranteeing a fulfilment of 50% of the request within 15 seconds and maintaining the power deviation up to 1 hour. Finally, an aggregation strategy with reduced communication requirements is formulated and the capability of following power requests from the system operator is verified by extensive simulations. The aggregated behaviour does not present consumption synchronization issues because the low-level controller is a PID strategy without cycling phenomena.

The rest of the paper is organized as follows. Section 2 describes the TER components and an analytical model, validated through experimental data. Section 3 explains the flexibility that a set of TERs can have in power demand, defines the energy service, and presents the proposed aggregator architecture. Finally, the last section shows the conclusions and future research directions.

2. ThermoElectric Refrigeration Unit

2.1. TER current uses

The interest in the development of TER units is increasing due to a multitude of positive existing aspects [33] that overcome the drawbacks they have when compared to Vapour-Compression Refrigerators (VCR), such as the lower Coefficient Of Performance (COP) and higher costs [34]. In particular, the advantages of TER units are utilisation of electrons as eco-friendly refrigerant without harmful environmental effects, being an ecological unit, simple design, light-weight, operation in any position, high reliability, low vibrations, noiseless operation, absence of moving parts leading to less maintenance demands, operation in severe environments, controllability within ± 0.1°C, temperature stability and small size [35, 36].

Precise temperature control, required for foodstuff preservation, is possible thanks to the high controllability of the electric current [35]. Solutions with ThermoElectric Cooler (TEC) modules are very popular for applications in different niche markets where size and other advantages make them attractive, like hotel room refrigerators (preferred for their silent operation), domestic refrigerators, refrigerators for mobile homes, recreational vehicles, cars, trucks, portable picnic coolers, and food-service refrigerators for airborne [37]. Applications in humanitarian contexts have been proposed as well [38].

A TER unit is supplied in Direct Current (DC) and, when the electrical grid operates in Alternating Current (AC), an AC/DC converter is needed to provide the DC supply. However, in some applications, the TER unit has the advantage that can be powered directly by DC electrical sources like Photo-Voltaic systems or batteries, being more economical and efficient than AC-supplied refrigerators [39, 40].

2.2. Components of a TER unit

A TER unit is composed of different parts (as shown in Figure 2):

- a thermally insulated cabinet (in which the temperature has to be lower than the ambient temperature);
- a ThermoElectric Cooler (TEC);
- heat exchangers at each side of the TEC device, and;
- one or more electric fans powered by the same external power supply that powers the TEC.

The fans force an air-flow over the dissipator inside and outside the cabinet as depicted in Figure 2. Moreover, the TEC module is composed of the union of some thermoelectric elements of N- and P-type. The thermoelectric elements are connected thermally in parallel, to ensure that one side of the TEC is hot while the other is cold when the TEC is powered. The thermoelectric elements are electrically connected in series through copper strips, to enable the electric current flowing through their legs. Furthermore, the thermoelectric elements are sandwiched between two ceramic plates of aluminum oxide, which isolate the TEC electrically from both heat exchangers. These ceramic plates are considered suitable conductors from the thermal point of view.

The TEC module is located within the TER insulation. The TER insulation has a variable thickness that depends on the TER capacity. Heat is pumped from the cold side

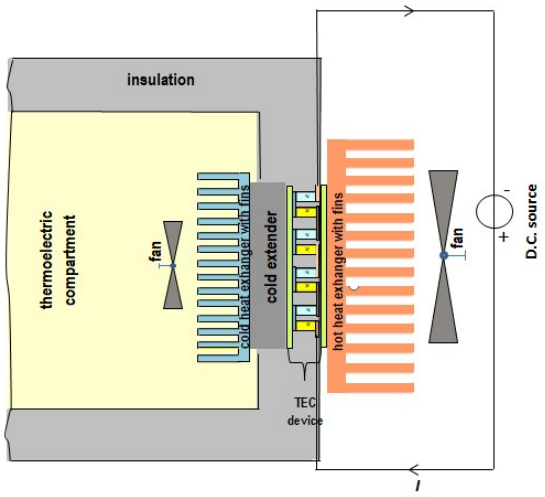

Figure 2: Schematic of the TER unit.

of the TEC to its hot side through charge carriers (electrons or holes) when a DC electric current supplies the module. Then, heat is transferred against the temperature gradient with the consumption of electrical energy. The heat flow causes the hot side to warm up and the cold side to cool down, requiring head exchangers on both sides.

Two heat exchangers are attached to the TEC module. The interior heat exchanger, made of aluminium finned heat sink, is fixed to a cold extender that in turn is attached to the cold side of the TEC. The role of the cold extender is to minimize the thermal bridges during the off periods of the TEC that would decrease the TER efficiency [41, 42]. This heat exchanger is useful to transfer the cooling effect from the cold side of the TEC to the thermoelectric compartment. Different configurations of heat exchangers can be used, see e.g., [43]. The electric fan installed on the cold heat sink is useful to provide forced convection for circulating cold air inside the compartment [33]. The heat exchanger outside the TER is installed on the hot side of the module to dissipate the heat into the environment. The finned heat sink is the most conventional heat exchanger, but sometimes it does not allow to obtain the desired performance. Other types of heat exchangers used on the hot side of TECs like heat pipe and water–air are presented in [41]. A fan installed at the hot side is useful to regulate the air flowing through the fins of this heat sink.

2.3. Analytical TER model

In order to determine the TER potential as a flexible load, a model reproducing its dynamics is built. Currently, in the literature it is possible to find models that represent the thermal operation of the TEC module [36, 44, 45]; however, there is no standard model able to reproduce the dynamics of the complete TER for control purposes. For this reason, this subsection presents the proposed dynamic model of a TER, whose parameters have been set up through experimental data. Table 1 presents the analogy between the electrical quantities and thermal counterparts for developing the model.

Table 1: Analogy between the Electrical Quantities and Thermal Counterparts.

Thermal quantity	**Units**	**Electrical quantity**	**Units**
Temperature T	K	Electric potential U	V
Absolute zero	0 K	Ground potential	0 V
Heat Flow Rate $\dot{Q}$	W	Electric current I	A
Thermal capacity C_t	J/K	Electrical capacitance C_e	F
Thermal resistance R_t	K/W	Electrical resistance R_e	Ω

Regarding the TEC module, the thermal operation model considered is presented in Eq. (1) and Eq. (2) (from [36, 44, 45]). A heat flow rate $\dot{Q}_c$ is absorbed by the TEC, as shown in Eq. (1), whereas a heat flow rate $\dot{Q}_h$ is delivered from the TEC module to the hot side sink, with magnitude given by Eq. (2).

$$\dot{Q}_c = \alpha T_c I_p - \frac{1}{2} I_p^2 R_p - K_p \Delta T, \tag{1}$$

$$\dot{Q}_h = \alpha T_h I_p + \frac{1}{2} I_p^2 R_p - K_p \Delta T, \tag{2}$$

where $\Delta T{=}T_h - T_c$.

Note that the heat flows depend on the electric current I_p, flowing through the module and the temperature of both plates, T_c and T_h.

Figure 3 shows a scheme of the electrical behaviour of the TEC module. Note that the consumed electric power is:

$$P = V_{in} I_p, \tag{3}$$

while the current I_p is determined by the difference between the input voltage V_{in} and the Seebeck effect voltage V_α by considering the Peltier electrical resistance R_p:

$$V_{in} - V_\alpha = I_p R_p. \tag{4}$$

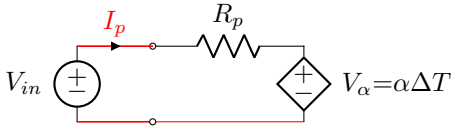

Figure 3: Electrical TEC module scheme.

The equivalent scheme of a TER is shown in Figure 4. In the scheme, the ambient temperature T_{amb} is a (possibly time-variant) parameter. The TER considers the internal compartment as a volume with temperature T_c and capacitance C_{TR}, isolated from the ambient temperature through a resistance R_{TR}, which represents the equivalent quantities for the internal parts of the TER (e.g. cold heat sink, cold extender, and insulated walls). The TEC module extracts heat from it at a rate $\dot{Q}_c$. Capacitance C_d and resistance R_d model the loads inside the TER (e.g. bottles of water or food stored), which are controlled by the

switch s. The outer environment of the TER, formed by the external plate and the heat sink is modelled as a mass with temperature T_h and capacitance C_{out}. It receives a heat flow $\dot{Q}_h$ from the TEC module while dissipates heat to the the ambient through a thermal resistance R_{out}. The parameters of the equivalent TEC module circuit are identified in such a way that they are consistent with the equivalent thermal equations according to the thermal-electrical analogy presented in Table 1.

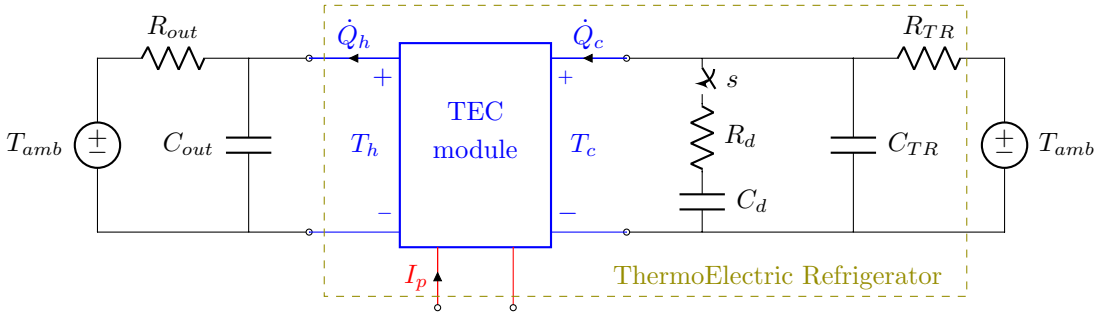

Figure 4: Equivalent scheme of a TER unit.

The dynamics of the cold $T_c(k)$ and hot $T_h(k)$ temperatures of the TER are given by Eq. (5) and Eq. (6), respectively, where k is the discrete time slot. Notice that the switch s is assumed open in these energy balances.

$$T_c(k) = \frac{T_{amb}(k-1) - T_c(k-1)}{C_{TR}R_{TR}} - \frac{\dot{Q}_c(k-1)}{C_{TR}} \tag{5}$$

$$T_h(k) = \frac{T_{amb}(k-1) - T_h(k-1)}{C_{out}R_{out}} + \frac{\dot{Q}_h(k-1)}{C_{out}} \tag{6}$$

2.4. Experimental data

In order to estimate the parameters of the TER model (α, K_p, R_p, R_{TR}, C_{TR}, R_{out}, and C_{out}) described previously (see Figure 4), experimental measures were recorded in a commercial TER. Figure 5 presents the actual TER unit used in this work.

The TER has a width of 0.42 m, a length of 0.42 m, and a height of 0.50 m. The internal capacity of the device is 42 l, and contains an insulation compartment with the bottom and upper thickness of 0.06 m, while the lateral thickness is 0.04 m. The device has two air fans: the first is inside, while the external one is mounted on the rear side of the appliance on the hot side heat sink. The unit has a rated power of 50 W [38]. The original internal electronic board, containing the power supply and the control system, has been disconnected and the TER has been supplied by a controllable AC/DC supply (see Figure 6). The on/off control system of the TER provided by the manufacturer has been replaced with the one developed by the authors, in order to achieve a control that needs less energy (the comparison between the control systems has been shown in [31]).

Figure 6 shows the block diagram of the hardware implementation and its components for measuring and controlling the TER. The datalogger is an Arduino device, and is connected

Figure 5: Actual TER used in the study.

to a computer that runs Simulink. The details of the implementation are reported in [31]. The system is powered by an AC/DC converter that takes energy from the power grid. A controllable DC/DC converter feeds the TER module. This converter is capable of regulating the voltage between 0 V and 32 V and can deliver up to 5 A. A Hall-effect current sensor S_C with a sensitivity of 185 mV/A monitors the current injected to the TER. A sensor S_V measures the voltage delivered to the TER. Both measurements, S_C and S_V, are sent to an Analog-Digital Converter (ADC) of a Data logger and allow to monitor the power consumed by the TER. The sample time is 1 s.

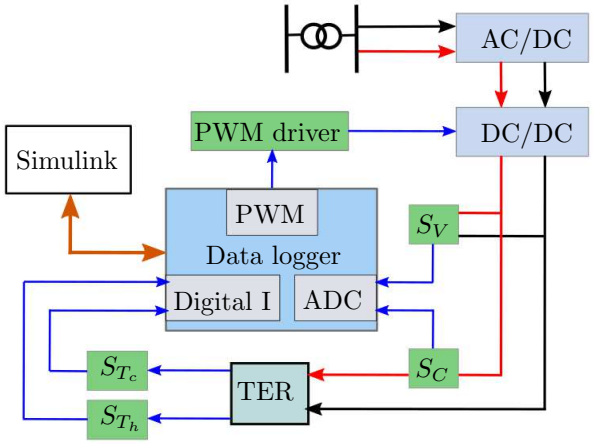

Figure 6: Block diagram of the implementation.

Temperatures T_c and T_h are measured with thermistor type sensors (sensitivity of 0.1°C), S_{T_c} and S_{T_h}, respectively. Both measurements are sent to the Digital inputs of the Data logger. All the information arriving at the Data logger is sent to a computer with Matlab-Simulink, by serial communication. The controller implemented in Simulink delivers a Pulse-Width Modulation (PWM) signal through the Data logger to the PWM driver to fix the voltage supplied to the TER by the DC/DC converter, allowing to implement feedback

control strategies. The driver is developed by a low-pass active filter.

It is highlighted that the measurements were carried out in a temperature-controlled chamber, and thus T_{amb} was the same in all measurement time, i.e., T_{amb}=18°C. Three different measurement sets were obtained with different input conditions i.e.:

- Experiment 1, by applying $V_{in,1}$=10.68 V;
- Experiment 2, by applying $V_{in,2}$=8.64 V;
- Experiment 3, by applying $V_{in,3}$=6.56 V.

For each experiment, the test started when T_c=T_h=T_{amb}, and V_{in}=0 (hence, I_p=0). Then, after one minute, V_{in} was set to the voltage defined in the experiment (1, 2, or 3). This voltage was kept for 4 h, that is the time required for T_c to reach equilibrium; after that, the voltage supply is turned off and the data acquisition continued for 5 more hours, enough time for achieving T_c=T_{amb} again. Figure 7 shows the behaviour of T_c, T_h, and T_{amb} for the three experiments. In Figure 7b, current I_p and voltage V_{in} are reported.

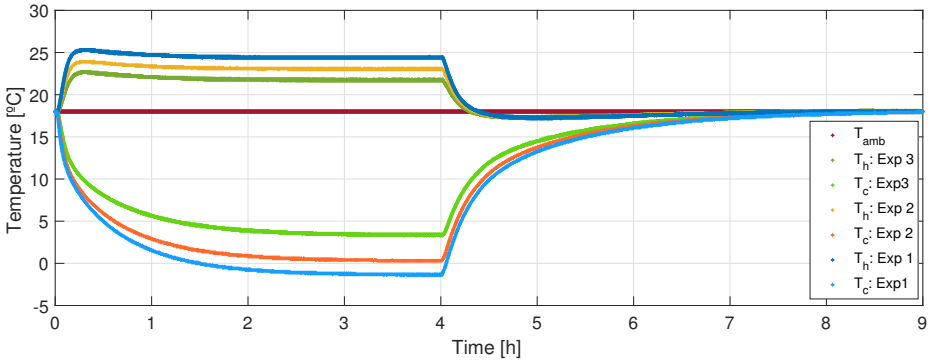

(a) Measurements of temperatures T_c, T_h, and T_{amb} during the 3 experiments.

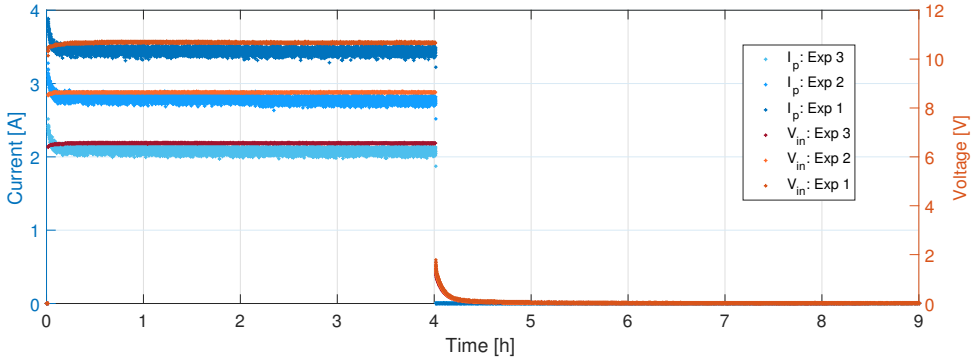

(b) Measurements of current I_p and voltage V_{in} during the 3 experiments.

Figure 7: Measurements for Experiment 1, 2 and 3.

2.5. TER parameters characterization

This subsection shows the methodology employed to obtain the TER parameters α, K_p, R_p, R_{TR}, C_{TR}, R_{out}, and C_{out} (see Figures 3 and 4). It is worth noting that the values of the parameters change depending on the TER under test; however, the procedure presented bellow can be applied as it is to any other TER. The parameters are calculated in three steps, as detailed in the following.

2.5.1. Step 1. Electrical parameters

The first step aims to obtain α and R_p from the experimental data of the three experiments. The Seebeck voltage can be obtained by cutting off the current I_p and measuring instantaneously the residual voltage, i.e.:

$$V_\alpha = V_{in} \mid_{I_p=0} . \tag{7}$$

Then, the Seebeck parameter α is determined as:

$$\alpha = \frac{V_\alpha}{\Delta T}. \tag{8}$$

Finally, considering only the electrical part of the TEC module, the module electrical resistance can be computed as:

$$R_p = \frac{V_{in} - \alpha \Delta T}{I_p} \tag{9}$$

Figure 8 shows the Seebeck voltages V_α for the experiments when V_{in} is turned off (after 4 h in Figure 7b). The purple asterisks (*) plotted on the curves represent the TEC voltage measurements one step after switching V_{in} off.

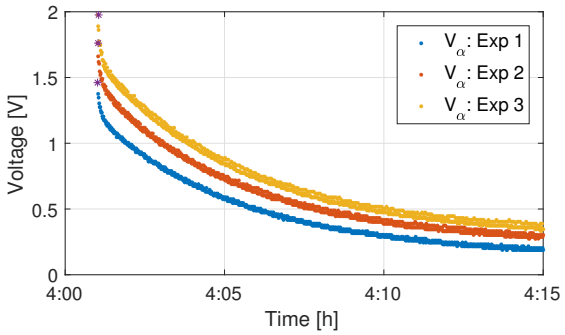

Figure 8: Experimental V_α.

Table 2 presents the resulting values for V_α and ΔT, aiming to compute α in each experiment; while the computed R_p takes into account V_{in}, I_p, and ΔT and is obtained as a mean value. It is noticed that R_p and α are consistent for the three experiments.

Table 2: Experimental values of V_α and ΔT, and computed values for α and R_p.

Experiment	V_α [V]	ΔT [°C]	α [V/K]	R_p [Ω]
1	1.98	25.8	0.0766	2.55
2	1.76	22.8	0.0773	2.54
3	1.46	18.3	0.0798	2.50
Mean value			**0.0779**	**2.53**

2.5.2. Step 2. Interior compartment thermal parameters

The second step aims to calculate the parameter K_p, C_{TR}, and R_{TR} through an optimization problem minimizing the Root Mean Squared Error (RMSE) between the measured temperature $\tilde{T}_c$ and the temperature T_c predicted by the model for the given voltage V_{in} and external plate temperature T_h.

The following equation reports the proposed optimization problem formulated to estimate the set of parameters:

$$\min_{K_p, C_{TR}, R_{TR}} \quad \sum_{j=1}^{J} \sum_{k=1}^{N} \left(T_{c,j}(k) - \tilde{T}_{c,j}(k) \right)^2 \tag{10a}$$

$$\text{s.t.} \quad T_{c,j}(k) = \mathfrak{f}(T_{c,j}(k-1),\ T_{amb}(k-1),\ \dot{Q}_{c,j}(k-1); K_p, C_{TR}, R_{TR}) \tag{10b}$$

$$\tau_{c,min} \leq C_{TR} R_{TR} \leq \tau_{c,max} \tag{10c}$$

$$0 < K_p,\ C_{TR},\ R_{TR} \tag{10d}$$

where J=3 is the number of the experiments, j refers to the considered experiment (i.e., j=$\{1, 2, 3\}$), and N refers to the experiment data length (i.e., N=32,400 s equivalent to 9 h, as shown in Figure 7).

The dynamic constraint in Eq. (10b) corresponds to the dynamic behaviour of T_c, where $\mathfrak{f}(\cdot)$ is defined as the right hand side of Eq. (5), evaluated using the measurements of I_p, T_h and T_{amb} for each experiment, while R_p and α are the mean values of the estimates for the 3 experiments in Table 2, and K_p, C_{TR}, R_{TR} are the decision variables of the optimization problem. The lower and upper bounds of the non-linear constraint (Eq. (10c)) are the minimum and maximum expected time constants of T_c when the system is cooling down, i.e., $\tau_{c,min}$=1179 s and $\tau_{c,max}$=2506 s. The optimization problem is solved in MATLAB®, by using the Sequential Quadratic Programming solver *fmincon function*. The optimal parameters are shown in Table 3. Note that the nonlinear constraint is fulfilled, obtaining τ_c=$C_{TR}R_{TR}$=2282 s.

Table 3: Optimal values for the TER parameters.

Parameter	**Value**	**Units**
K_p	0.134	W/K
C_{TR}	6300	J/K
R_{TR}	0.362	W/K
C_{out}	4500	J/K
R_{out}	0.072	W/K

2.5.3. Step 3. External equivalent model parameters

In order to calculate the outer plate thermal parameters C_{out} and R_{out}, the following optimization problem is formulated:

$$\min_{C_{out},R_{out}} \quad \sum_{j=1}^{J}\sum_{k=1}^{N}\left(T_{h,j}(k)-\tilde{T}_{h,j}(k)\right)^2 \tag{11a}$$

$$\text{s.t.} \quad T_{h,j}(k)=\mathfrak{f}\left(T_{h,j}(k-1),\ T_{amb}(k-1),\ \dot{Q}_{h,j}(k-1);C_{out},R_{out}\right) \tag{11b}$$

$$\tau_{h,min}\leq C_{out}R_{out}\leq\tau_{h,max} \tag{11c}$$

$$0<C_{out},\ R_{out} \tag{11d}$$

The aim is to obtain the values of C_{out} and R_{out} that minimize the RMSE between the modelled T_h and the experimental $\tilde{T}_h$ temperatures. This problem is developed with the same structure of the problem in Eq. (10). Constraint Eq. (11b) corresponds to the dynamic behaviour of T_h, where $\mathfrak{f}(\cdot)$ is defined as the right hand side of Eq. (6), and C_{out} and R_{out} are the decision variables of the optimization problem. However, K_p is a known parameter and T_c is taken from the TER experimental measurements. Moreover, $\tau_{h,min}$=267 s and $\tau_{h,max}$=564 s. the resulting parameters are shown in Table 3. The nonlinear constraint is fulfilled, obtaining τ_h=$C_{out}R_{out}$=323 s.

2.6. Model validation

In order to validate the proposed model, simulations with all the obtained parameters are developed and compared with the experimental data. Figure 9 shows the T_c and T_h responses of the model for the three experiments.

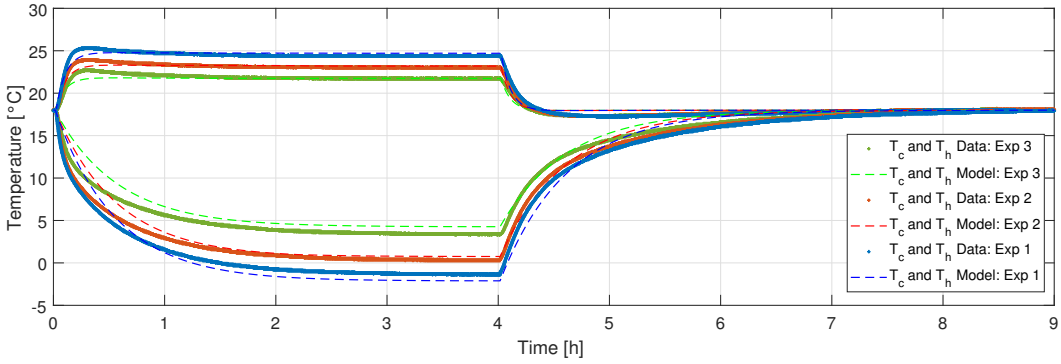

Figure 9: Temperature validation for the experiments.

Table 4 reports the characterization of the error of the estimated model for T_c and T_h. The RMSE and Maximum Absolute Error (MAXAE) are reported. Notice that the RMSE is lower than 1°C, also considering transient conditions for the inner temperature and lower than 0.4°C for the external temperature. The maximum deviation is observed for T_c at the beginning of the tests, when T_c is above 10°C, out of the operation range. It can

be seen from Figure 9 that there is no systematic bias in the model output along all the experiments. It can be concluded that the model is suitable to properly represent the system for consumption analysis and control design.

Table 4: Error measures for the TER model.

Exp	T_c		T_h	
	RMSE [°C]	MAXAE [°C]	RMSE [°C]	MAXAE [°C]
1	0.92	3.3	0.38	0.8
2	0.86	3.4	0.33	0.7
3	0.94	2.9	0.36	0.7
Mean	**0.91**	-	**0.35**	-

2.7. Low level control

In a TER the voltage applied to the TEC module is manipulated to achieve a desired internal temperature [38]. Note that the control of the interior temperature is more accurate than the one reachable by VCRs with a single-speed compressor. Only VCRs that contain variable speed compressors and electronic expansion valves can provide high accuracy temperature control [33].

The TER temperature can be controlled by different strategies, see e.g. [46, 47]. For example:

- *ON/OFF* controller: it is a simple strategy where the power supply is either at maximum voltage or turned off, maintaining the temperature oscillating inside a predefined hysteresis band. During the ON cycle, when the supply is at maximum voltage, the temperature difference between the hot and cold sides of the TEC modules is also maximum, increasing the consumption and representing a drawback in the system. Another drawback is that, when the TEC module is switched off, a significant amount of heat gathered at the external heat sink returns into the TER, forming a thermal bridge. Efficiency can be improved by applying a low voltage during the OFF cycle.

- *Proportional-Integral-Derivative* (PID) controller: In this strategy the voltage is varied smoothly between 0 V and the maximum. The instantaneous voltage is obtained by a feedback law that operates on the error or difference between the actual temperature and the desired one (set-point). The PID control action C_{PID} follows the equation:

$$C_{PID}(t) = k_{pr}e(t) + k_i \int_0^t e(t')dt' + k_d \frac{de(t)}{dt}, \tag{12}$$

  where k_{pr}, k_i, and k_d denote the coefficients for the proportional, integral, and derivative terms.

  If the controller parameters are properly selected, the feedback operation of the system will find the required voltage to reach the desired temperature, leading to a low energy consumption.

In [31], the authors have shown a comparison between ON/OFF and PID strategies for the TER system modelled in the previous subsections, highlighting the experimental superior

performance of the PID solution without derivative action, i.e., $k_{pr} = -1.804$, $k_i = -0.0017$, and k_d=0. To determine these PID controller coefficients, a first-order model with delay of the T_c response is estimated; then, considering the MATLAB *Control System* toolbox, the coefficients are computed, fulfilling an overshoot effect lower than 5%, a settling time lower than 3145 s, and a control signal range lower than 2 V when a temperature change of 1°C is requested. The experimental results have shown that the power of the ON/OFF solution exhibits a switched behaviour, while the PID controller presents a smooth behaviour. With the PID it is easier to follow a power deviation request, given that the power profile can be modified (upward or downward) without affecting significantly the cold temperature T_c, i.e., it can be treated as a flexible load. Moreover, the disturbance time of the PID strategy is significantly lower than the one of the ON/OFF strategy, and the PID strategy has also an energy saving of 43% with respect to the ON/OFF strategy.

3. Flexibility and TER Aggregation Strategy

In this section, the flexibility in energy consumption of a set of TERs is evaluated. Then, an aggregation strategy is proposed in order to provide balancing services to the electrical grid. It is shown that power demand of TERs can deviate from nominal values while keeping the system in normal working conditions, by modifying the internal set-point temperature (the set-point temperature is the target value of the controlled temperature that has to be maintained by the control strategy). Moreover, it is proposed an aggregator that manipulates the set-points of a set of TERs to follow up/down power requirements from the System Operator (SO).

3.1. European electricity balancing services.

This subsection presents a brief recall of the energy balance services usually adopted by SOs in Europe. These SOs use different processes and products to balance the system and restore the frequency. In this sense, the Commission Regulation (EU) 2017/2195 of 23 November 2017 [48] sets up the requirements for the technical parameters of standard products in order to facilitate the exchange of balancing energy across borders.

The standard structure is presented in Figure 10. The preparation period is the time required to receive the signal and activate the service. Then, there is a ramp-up period, followed by the delivery period, and finally the ramp-down period. The request for the ramp-down period is not specified in the current versions of the rules. Indicatively, the ramp-down period can be similar to the full activation time. The technical parameters of the standard structure are aligned with operational flexibility indicators presented in studies such as [49] and [50], where the defined metrics are the power provision capacity, power ramp-rate capacity, and ramp duration. Notice that these indicators can be obtained with the information in Figure 10.

Considering the guideline on electricity balancing, presented by the Commission Regulation [48], the balancing energy services in Europe are organised as:

- *Frequency Containment Reserves* (FCR): The active power reserves available to contain system frequency after the occurrence of an imbalance. During the ramp-up period, it requires the delivery of 50% of the reserve within 15 s, and 100% within 30 s. The

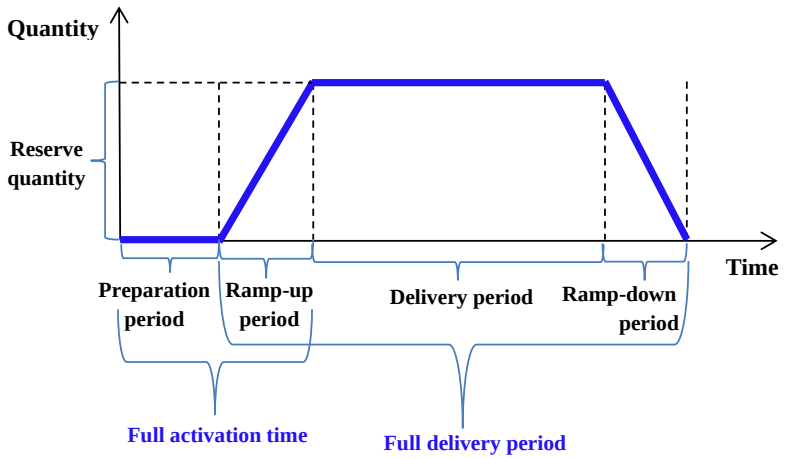

Figure 10: Standard structure of balancing services provision.

FCR rules also specify that this delivery should be sustained for 15 min. In addition, the FCR must have automatic activation [51].

- *Frequency Restoration Reserves* (FRR): The active power reserves available to restore system frequency to the set point and, for a synchronous area consisting of more than one load-frequency control area, to restore power balance to the scheduled value. The standard FRR can by activated manually [52][2] or automatically [53][2]; the full activation time for the first one shall be 12.5 min, while for the second is 5 min. Moreover, for both FRR services, the delivery should be for 15 min.

- *Replacement Reserves* (RR): The active power reserves available to restore or support the required level of FRR to be prepared for possible additional system imbalances. The full activation time of the RR service is 30 min, considering the preparation and the ramp-up periods from 0 to 30 min. Moreover, the duration of the delivery period is between 15 min and 60 min; whereas, the activation of the service is scheduled with manual activation [54][2].

It is worth to note that the full activation time has to be considered as the maximum allowed time to deliver the different services. Besides that, no specific shape in the ramp-up period is required by the current version of the regulatory framework. On these bases, it is possible to indicate that:

1. the most challenging ramp time period is the one referring to FCR. Thus, the fulfillment of this time cover also the ones related to all the other services (FRR and RR).
2. The delivery periods of FRR and FCR are equal: so, the fulfillment of the FCR delivery period covers also the one related to FRR.

[2]At the current stage, the specifications referring to FRR and RR are still under development. The technical characteristics have to be considered as the ones currently available on the official ENTSO-E website

3. The most challenging delivery time is instead the one referring to the RR service.

Thus, Section 3.3 shows the capability of a set of TERs to provide all the services through two sets of simulation: the first one, based on the FCR requirement, will cover both FCR and FRR, whereas the second one will verify the compliance of the TERs performance with the RR specifications.

3.2. Flexibility analysis

The analysis of the flexibility in energy consumption of a set of TERs set is performed evaluating the following characteristics:

1. The power modification when there is a temperature set-point change.
2. The time required for the TER to achieve equilibrium after a temperature set-point change.
3. The service that a set of TERs can provide to the electrical grid.

Hence, a set of simulations have been developed with the purpose of evaluating these three characteristics. Power demand P, cold temperature T_c and stabilization times are thus assessed.

Considering the TER controlled temperature, the standard temperature set-point used for domestic thermoelectric refrigerators is 5°C [35, 55, 56]. It must not fall below 0°C to avoid the presence of frost inside the cabinet [42]; and according to common standards such as the EC Regulation 852/2004 [57], the regulation of the Food Standards Agency (FSA) in the UK [58], and the Essential food safety practices of the Food Standards Australia New Zealand (FSANZ) [59], the chilled food storage inside the cabinet must not exceed 8°C; therefore, the TER set-point is modified to $T_{sp,down}$=2°C when a power demand increment is required, and to $T_{sp,up}$=8°C when a power demand reduction is requested, in order to evaluate the power modification when there is a temperature set-point change. It is worth noting that, in general, the choice of the temperature set-points depends on the user's preferences.

The behaviour of 50 TERs is evaluated for different conditions of cold temperature set-point $T_{c,sp}$, capacitance C_{TR}, ambient temperature T_{amb}, and disturbances (parametrized by s, C_d and R_d, see Figure 7). Each test lasts 5 h and starts with the TER controlled in equilibrium, i.e., T_c=T_{sp}. In particular, T_{sp} is randomly selected from the set $\{3, 4, 5, 6, 7\}$°C with uniform probability. T_{amb} is selected randomly for each TER and for each T_{amb} a random walk strategy is performed by varying it within ±1°C each hour. For C_{TR}, three TER sizes are analysed, 42 l (which was previously assessed), 30 l and 60 l; with associated thermal capacitance of 6300 J/K, 4600 J/K, and 9300 J/K, respectively.

Regarding the disturbances, during the test each TER is perturbed with masses (representing food) at ambient temperature. C_d and R_d are tuned to represent bottles of water containing 0.5-1 l that can be introduced/removed from the TER up to 10 times during the simulation, as described in [31]. Table 5 summarizes the range of variation for each parameter.

3.2.1. PID-controlled TER flexibility evaluation

In the first set of simulations, a temperature set-point change is executed for the 50 TERs considering the PID controller presented in the subsection 2.7. For example, one TER temperature response is shown in Figure 12. This simulation is run two times:

Table 5: Intervals of model parameters for setting the simulations

Parameter	Minimum	Maximum	Units
$T_{c,sp}$	3	7	°C
T_{amb}	18	26	°C
C_d	8000	58400	J/K
R_d	0.35	0.75	W/K

- the first time it is made by changing the set-point to $T_{sp,down}$ (see Figure 12a green line).
- the second time it is made by changing the set-point to $T_{sp,up}$ (see Figure 12a blue line).

Figure 12b depicts the TER power demand, for the set point changes $T_{sp,up}$ and $T_{sp,down}$. Before a set-point variation, this TER is consuming on average 16.86 W. Then, when $T_{sp,up}$ is applied, the power (blue line) reduces to 1.10 W instantaneously (i.e., 93.5% reduction); further on, the power stabilizes after 2580 s (43 min) consuming on average 9.89 W (i.e., 58.7% reduction). Likewise, when $T_{sp,down}$ is applied, the power (green line) increases to P_{max}=38.90 W instantaneously (i.e., 230.7% increment) and remains there for a few seconds; further on, the power stabilizes after 2640 s (44 min) consuming on average 26.40 W (i.e., 156.6% increment). Small oscillations are observed when perturbations increase/decrease the thermal capacitance of the system.

Therefore, it is noticed that changing the temperature set-point, the system can either reduce or increase its demand instantaneously and could provide balancing services such as FCR, FRR and RR. However, considering the results with PID controller, the duration for which the TER maintains the power at zero or P_{max} is not enough to comply with the required delivery time. Then, a modified controller is proposed to provide a reliable energy service.

3.2.2. Modified PID controller

The PID controller has been thus modified with the purpose of increasing the interval length when P=0 or P=P_{max} after a set-point change. Figure 11 shows the block diagram of the proposed modified control strategy. A new variable β is defined to change the set-point. It only considers three possible states for each TER:

- 0: Nominal operating set-point, i.e., $T_{sp,nor}$ which is defined from the set $\{3, 4, 5, 6, 7\}$°C;
- 1: High set-point, i.e., $T_{sp,up}$=8°C;
- -1: Low set-point, i.e., $T_{sp,down}$=2°C.

The Modified control block aims to saturate the controller action when a set-point change command arrives. This modification allows the TER to achieve the new set-point faster than with the PID controller and also maintains the power at zero or maximum power for a longer interval.

The algorithm (Alg_s block) identifies when a set-point change is requested, either to reduce (β goes from 0 to 1) or increase (β goes from 0 to -1) the demand, and saturates the

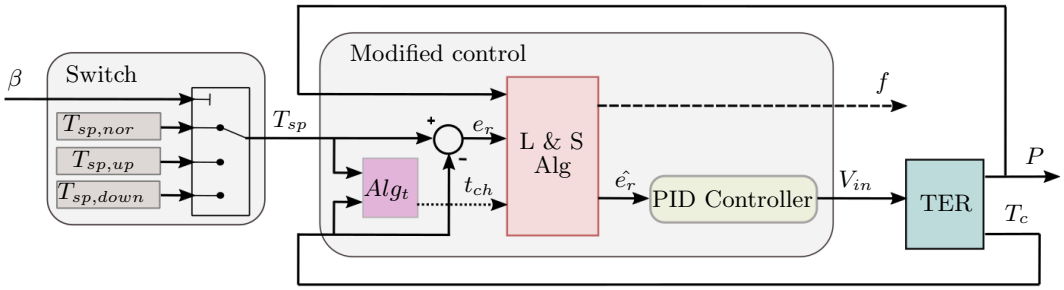

Figure 11: Modified TER control strategy.

controller output (V_{in}=0 to increase temperature or V_{in}=V_{max} to reduce it) while the TER reaches the new temperature set-point. The algorithm (L & S Alg block) also reports if the TER already achieved the new temperature. The variable f indicates the TER flexibility; f=1 signals to the aggregator that the system is not saturated and has the possibility to vary power demand, while f=0 signals a saturated controller without capacity to vary power demand. In fact, the aggregator needs f in order to select which TERs are able to modify their temperature set-points.

A second set of simulations evaluates the flexibility of TERs with the modified controller. The same conditions of the simulation campaign in subsection 3.2.1 are maintained, using the modified controller architecture instead of the PID controller. Figure 12a depicts the TER temperature when high (see red dashed lines) and low (see purple dashed lines) set-point changes are applied, while Figure 12b shows the power demand (see red and purple dashed lines).

3.2.3. Flexibility analysis

The modified PID controller allows achieving P=0, as well as P=P_{max} for a longer time interval than the one related to the PID controller. By considering the power reduction to P=0, the system can instantaneously reduce the demand by 100% and keeps this condition for 7 min; after that, the power stabilizes at the same value obtained when using the PID controller. This time does not fulfil the requirements for FCR provision. Considering a power rise to P=P_{max}, the system increases its demand instantaneously by 230.7%, and keeps it for 21 min. It is worth to note that this time matches with the requirements related to FCR and FRR service provision but not the RR service. In order to guarantee a proper compliance of the technical requirements of the balancing services, an aggregation strategy is introduced in Section 3.3.

Recall that the TERs evaluated in the simulation campaigns have different parameters (see Table 5), then, their time response to a set-point change varies. The histograms in Figure 13 illustrate this fact by reporting the number of TERs staying at maximum/zero power for given time intervals, for both control strategies. Note that even the same TER subject to different perturbations can stay different periods in saturated condition.

Figure 13a depicts the number of TERs that remain in P=0. It is noted that with the nominal PID controller, most of the TERs (92%) come back to consume power after 5 min or less and 8% after 5 ÷ 10 min, whereas with the modified controller, on average they stay

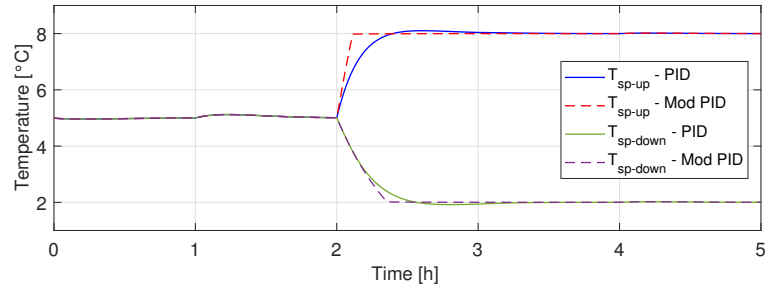

(a) TER temperature.

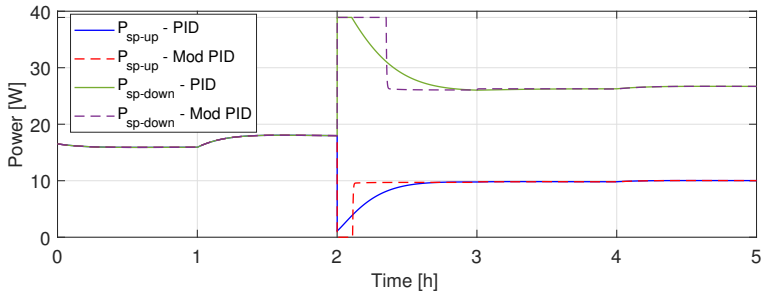

(b) TER power.

Figure 12: TER flexibility, with the PID controller and modified PID controller.

longer at $P = 0$ but they show more dispersion, 20% of the TERs resume their power after $0 \div 5$ min, 52% after $5 \div 10$ min, 24% after $10 \div 15$ min, and 4% remain more than 15 min. In the same way, Figure 13b shows that with the nominal PID controller just 18% of the TERs remains at $P{=}P_{max}$ for more than 15 min, whereas with the modified controller this number increases to 68%. Notice that not all TERs are reported in Figure 13b, because they remain longer than 1800 s (7 TERs for the PID and 17 TERs for the modified PID).

Summarizing, the considered TER systems equipped with the nominal PID controller cannot maintain their power at zero or P_{max} for a time long enough to provide FCR and FRR services. While, with the modified PID controller, the systems improve their ability to respond within the time frame specified for the regulation service. However, to properly exploit the above mentioned characteristics, an aggregator is required to synchronize the power deviations of the set by managing the temperature set-point of each TER, providing energy services to the SO.

3.3. TER Aggregator

This subsection proposes an architecture to offer balancing services, such as FCR, FRR and RR, with a set of TERs, through an aggregator that synchronizes the temperature set-point changes of the TERs. An automatic control strategy is proposed in order to reduce or increase the power demand of the set, taking advantage of the flexibility found in the previous sections.

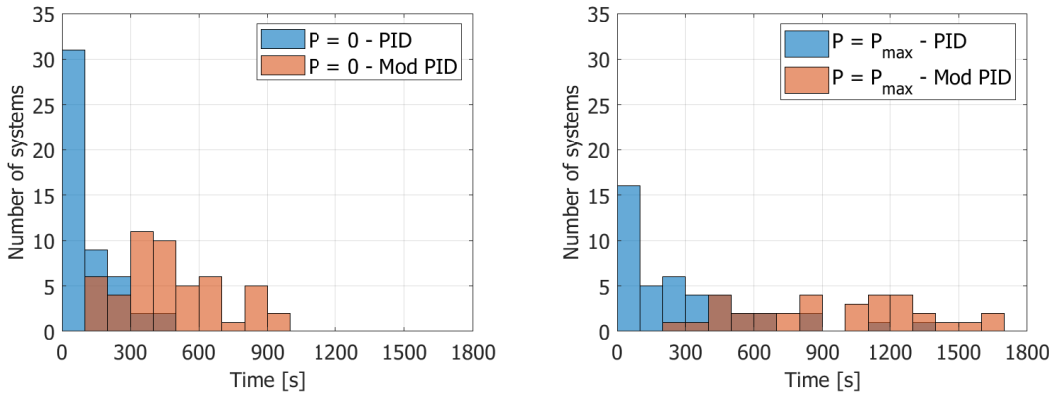

(a) $P = 0$. (b) $P = P_{max}$.

Figure 13: Histogram of the time elapsed consuming zero or maximum power after a set point change.

The aggregator is designed to respond to a SO requirement, assuming there is a signed contract with defined prices between the SO and the aggregator in order to provide the service. The number of TERs involved in the provision of flexibility is known in advance. Figure 14 shows the block diagram of the system, whereas Table 6 presents the information exchange between the aggregator and each TER.

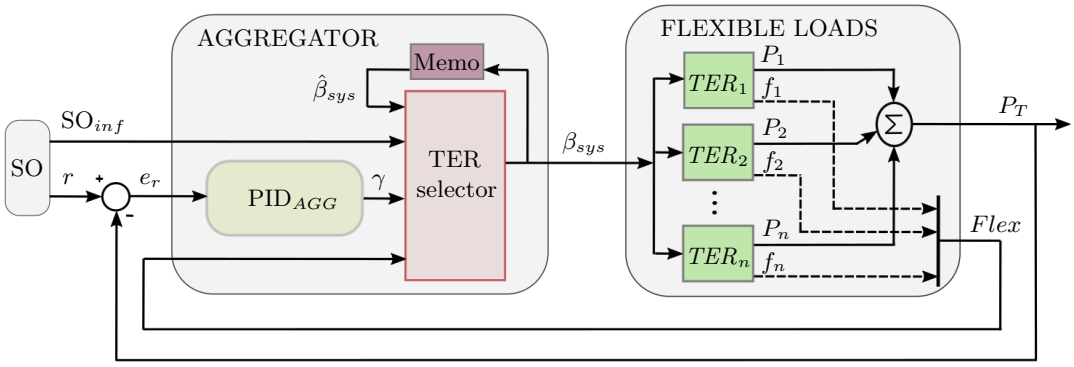

Figure 14: Block diagram of the TER aggregator.

When the SO makes a power deviation request (signal r), the aggregator must decide how many and which TERs must activate their flexibility to achieve the requested service and it must be performed within the established times. As the power demand and flexibility state of each TER vary with time, it is not a trivial task to select the subset that will offer the service. Then a feedback strategy is proposed.

The AGGREGATOR operates through two control actions, i.e., a PID controller (PID_{AGG}) and a TER selector. Both actions operate when a SO request arrives. The controller has a

Table 6: Information exchange between the aggregator and the TER units.

Message	Aggregator		TER unit	
	Variable	**Data type**	**Variable**	**Data type**
Send	β state	2 bits	Power P	Integer
			f state	Boolean

1 s sampling time, enough for accomplishing the system time response when providing the energy service (30 s in FCR service).

The output of the PID_{AGG}, signal γ, is the number of TERs that must change the set-point. A positive value indicates increasing the set-point, and a negative number the opposite. Thus, the output is saturated between $-n$ and n, where n is the number of TERs participating in the service provision.

The TER selector block is developed for deciding which TERs must change set-point to comply with the PID_{AGG} command. This selector follows the flow chart sequence presented in Figure 15. This sequence has two main logics, one for the power reduction request and another for the power increase. In both cases, the sequence looks for the TERs subset that has flexibility i.e., f=1, and can change the set-point to the value desired by the PID_{AGG}. The output β_{sys} contains the temperature set-point state of all the TERs, i.e., β_{sys}=$\{\beta_1,\ \beta_2,\ \ldots\ \beta_n\}$.

The FLEXIBLE LOADS block represents the set of TERs and provides as output the total electric power P_T of the set. It also collects the flexibility information f of all systems and reports the signal $Flex$=$\{f_1,\ f_2,\ \ldots\ f_n\}$ to the AGGREGATOR. Notice that the TER_i blocks presented in Figure 14 are considering not only the TER unit but also the modified PID controller and the switch, as depicted in Figure 11.

In order to calculate the PID_{AGG} parameters, a simulation with a set of n=100 TERs is developed. In this case, cold temperature set-point T_{sp}, capacitance C_{TR}, ambient temperature T_{amb}, and disturbances C_d and R_d are randomly generated as in the previous section.

First, the power demand of the aggregated set is analysed by modifying simultaneously the 100 TER temperature set-points to 1, i.e., β_{sys}=$\{1,\ 1,\ \ldots\ 1\}$ (activating downward flexibility). Secondly, it has been studied the plant (FLEXIBLE LOADS block) behaviour by modifying the 100 TER temperature set-points to -1, i.e., β_{sys}=$\{-1,\ -1,\ \ldots\ -1\}$ (activating upward flexibility). Figure 16 shows the plant response for both set-point modifications.

Then, two dynamic models of the plant behaviour are estimated to represent the upward and downward dynamics of the systems and a controller is derived. The models are linear and time-invariant in transfer function form, $G_{up}(s)$ and $G_{down}(s)$, expressed as:

$$G_{up}(s) = \frac{25.95s^2 + 0.017s + 9.3e^{-6}}{s^2 + 1.1e^{-3}s + 6.8e^{-7}} \tag{13a}$$

$$G_{down}(s) = \frac{-17.35s^2 - 0.018s - 3.6e^{-6}}{s^2 + 2.3e^{-3}s + 3.7e^{-7}} \tag{13b}$$

The quality of the models is measured evaluating the similitude of the models output

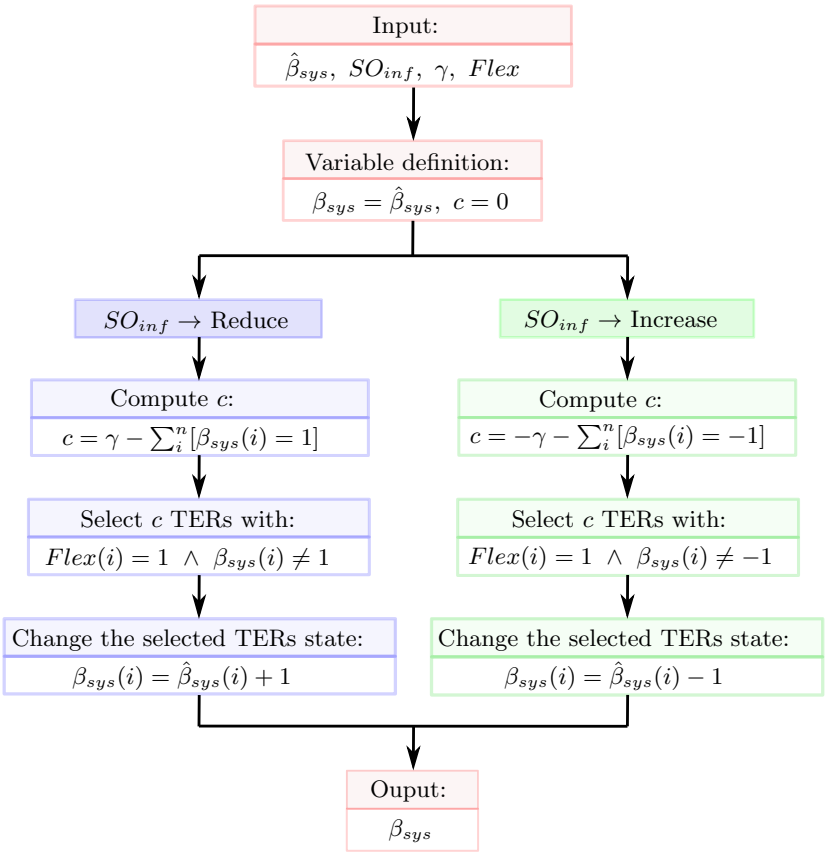

Figure 15: TER Selector sequence.

with the aggregated power obtained in the simulation, i.e., the FIT, defined as

$$FIT = 100 - \frac{\|x - x_{ref}\|}{N_s} 100(\%) \tag{14}$$

where x is the test data (i.e., the estimated model output), x_{ref} is the target data (i.e., the simulation response), and N_s is the number of samples.

The estimated models have FIT_{up}=93% and FIT_{down}=94%, respectively. This is accurate enough to design the controllers.

Considering the MATLAB *Control System* toolbox, a PID controller (see Eq. (12)) that works for both models ($G_{up}(s)$ and $G_{down}(s)$) is designed to stabilize the power in less than 25 s. The controller parameters are k_{pr}=0, k_i= − 0.012, and k_d=0.

The system is evaluated in several Demand Side Flexibility (DSF) plans for providing FCR, FRR and RR services, following the sequence: the SO sends to the aggregator the power that the set of TERs must consume for the following 15 min (FCR and FRR) or 1 hour (RR), this power can be lower or higher than the one in normal operation. Therefore, two sets

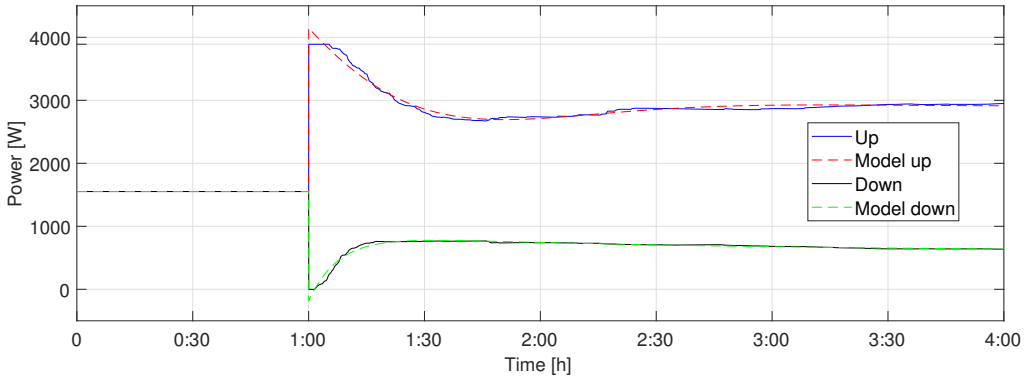

Figure 16: Models validation.

of experiments are developed for evaluating these energy services. For all experiments, cold temperature set-point T_{sp}, capacitance C_{TR}, ambient temperature T_{amb}, and disturbances C_d and R_d are generated randomly within the intervals in Table 5.

First, in the FCR service experiments, 8 different power levels (SO requests) are assessed. Moreover, following the FCR service specifications, the requested power must be delivered within 30 s after the SO request, and 50% of the requested power must be delivered within 15 s of the request arrival; while the ramp-down period must be lower than 5 min.

In Figure 17, the aggregator response for different power levels is presented. Figure 17a shows the deviations in the power demand following the SO requests. These power modifications are based on the nominal operation power i.e., the set of TERs has an average power of P=1540 W in nominal operation then, at the hour 1:00, the SO request arrives. This power request is supposed to be 37%, 50%, 75%, 125%, 150%, 175%, 200%, and 223% of the nominal power (i.e.,1540 W being 100%). The minimum and the maximum power requests, i.e., 37% and 223%, are found through repetitive simulations and they are related to the condition where the entire set of TERs has been involved in the FCR service provision (no more devices are available for further regulation). Therefore, the flexibility of the set of TERs allows the SO to request any power demand between 575 W and 3500 W for the next 15 min, i.e., the flexibility band for offering the FCR service is 2925 W. Besides, when the FCR service has finished, the aggregator recovers the power to the nominal one in 4 min avoiding any rebound effect, that is, there is no (positive or negative) peak in power demand at the end of the service, during the ramp-down period or later, see e.g. [25]. Notice that this aggregator response satisfies also the delivery period of the FRR service and the activation period can be regulated to a longer ramp-up time in order to fit the specified time of this service.

Figure 17b depicts the number of systems that are called to modify their temperature set-point, either upward (β_i=1) or downward (β_i=−1), i.e., the variable β_{sys} in each experiment. Then, at each time step, it is reported the number of TERs with temperature state in 1 for the SO requests higher that the nominal power, and in -1 for requests lower than the nominal power. It is shown how the aggregator responds to the SO request, modifying properly the temperature set-points of some TERs, reaching the requested power in less than 30 s and

maintaining it during 15 min for all the different power levels, meeting the FCR requirements.

Table 7 summarizes the results. For each SO request (r) are reported the average power effectively consumed during the delivery period ($\bar{P}$), the resulting percent error ($\bar{E}$), the standard deviation of the power demand (σ), the ramp-up times to the 50% ($t_{ru,50\%}$) and 100% (t_{ru}) of the capacity, the recovery time required by the 95% of the TERs for returning to the normal temperature set-point after the service ($t_{r,95\%}$), the recovery time required by the complete set of TERs (t_r) and finally the resulting ramp-up (ρ_u) and ramp-down (ρ_{dw}) rates. Note that the worst-case power deviation is 0.53%, all the power requests are achieved in less than 20 s, and half of the requests are fulfilled in less than 10 s. The standard deviation of the service is lower than 1% of the delivered power. The recovery time indicates the interval required to offer again the service. It can be seen that t_r is much longer than the delivery period and it varies widely with the offered power level. However, most of the capacity (i.e., 95%) is available after a shorter time $t_{r,95\%}$. This characteristic can be exploited by the aggregator to modulate its offer in successive time periods.

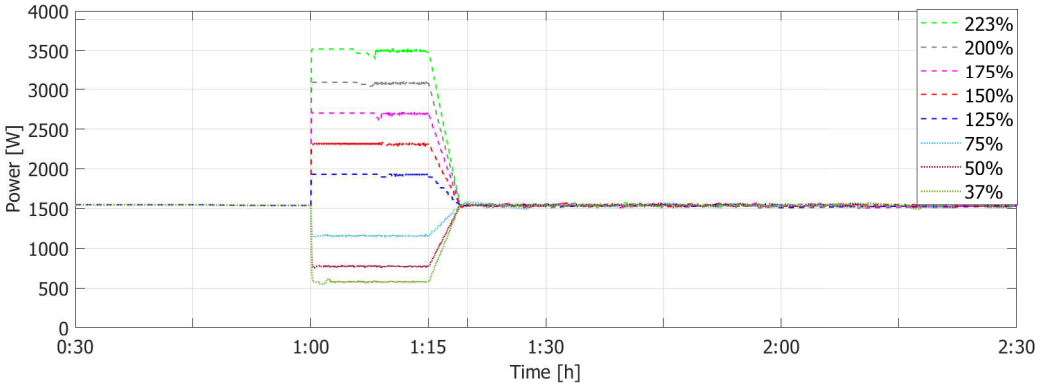

(a) Power consumed by all the TERs.

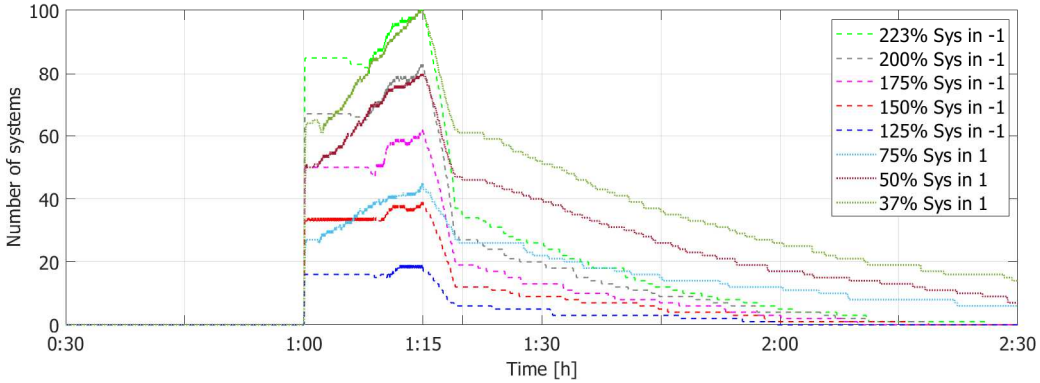

(b) Number of TERs changing the set-points.

Figure 17: Aggregator response for the Frequency Containment Reserve (FCR) service.

Table 7: Aggregator characteristics during the Frequency Containment Reserve (FCR) service.

r [W]	$\bar{P}$ [W]	$\bar{E}$ [%]	σ [W]	$t_{ru,50\%}$	t_{ru}	$t_{r,95\%}$	t_r	ρ_u [W/s]	ρ_{dw} [W/s]
3500	3498.0	0.06	23.8	5”	9”	39’44”	1h6’5”	217.8	-2.3
3080	3078.7	0.04	13.3	5”	9”	36’55”	58’48”	171.1	-1.8
2695	2694.0	0.04	17.5	5”	9”	32’57”	49’53”	128.3	-1.4
2310	2309.7	0.02	9.4	5”	9”	24’39”	55’57”	85.6	-0.9
1925	1926.9	-0.10	9.4	5”	8”	3’42”	39’29”	48.1	-0.5
1155	1156.6	-0.13	5.2	7”	18”	1h17’	2h5’	-21.4	0.5
770	772.6	-0.34	5.5	7”	15”	1h22’	2h51’	-51.3	0.9
575	578.1	-0.53	9.5	7”	17”	1h37’	3h24’	-56.8	1.2

Second, in the RR service experiments, 7 different power levels (SO requests) are assessed. Following the RR service specifications, the requested power must be delivered within 30 min after the SO request and must be maintained for 1 h.

In Figure 18a, the aggregator response for different power levels is presented. Figure 18a shows the deviations in the power demand following the SO requests. The power modifications are based on the nominal operation power. This experiment is carried out for 47%, 50%, 75%, 125%, 150%, 175%, and 185% of the nominal power. Therefore, the flexibility of the set of TERs allows to offer reserve capacities between 730 W and 2850 W for delivery periods of 1 hour, i.e., the flexibility band for offering the RR service is 2120 W. Notice that the capacity for this service is 805 W lower than for the the FCR one. Finally, no rebounds are generated at the end of the service.

Figure 18b depicts the number of systems that are called to modify their temperature set-point, either upward or downward, for each experiment. It is shown how the aggregator responds to the SO request, modifying properly the temperature set-points of some TERs, maintaining the power deviation during 1 hour for all the different power levels, meeting the RR service requirements.

Table 8 summarizes the results. The same characteristics evaluated in Table 7 for the FCR service are considered. It can be seen that the precision in power tracking is similar for both services. Also the ramp-up and recovery times are comparable. In this case, the ramp-up time to the 50% ($t_{ru,50\%}$) is not reported as the full ramp-up time t_{ru} is much lower that the limit of 30 min, defined for the RR service.

Thanks to the proposed control strategy, the aggregation of TERs is able to offer this service according to the specifications. The set of TERs considered in this paper covers partially the minimum reserve capacity required by the SO but the strategy can be scaled to manage a larger set of TERs. Thanks to the appropriate control actions, this paper demonstrates the possibility for the TERs to be compliant with real services defined in existing network code.

Table 8: Aggregator characteristics during the Replacement Reserve (RR) service.

r [W]	$\bar{P}$ [W]	$\bar{E}$ [%]	σ [W]	t_{ru}	$t_{r,95\%}$	t_r	ρ_u [W/s]	ρ_{dw} [W/s]
2850	2849.7	0.01	10.1	10”	37’2”	3h32’39”	131.0	-1.6
2695	2694.8	0.01	11.1	9”	35’6”	3h19’49”	128.3	-1.4
2310	2310.0	0.00	9.9	9”	22’38’	2h37’45”	85.6	-0.9
1925	1925.4	-0.02	10.5	8”	8’48”	1h33’37”	48.1	-0.5
1155	1155.2	-0.02	5.7	19”	1h5’25”	3h7’1”	-20.3	0.5
770	771.9	-0.24	7.8	15”	1h50’24”	5h54’28”	-51.3	0.9
730	736.5	-0.90	13.2	19”	1h52’23”	5h55’23”	-42.6	1.0

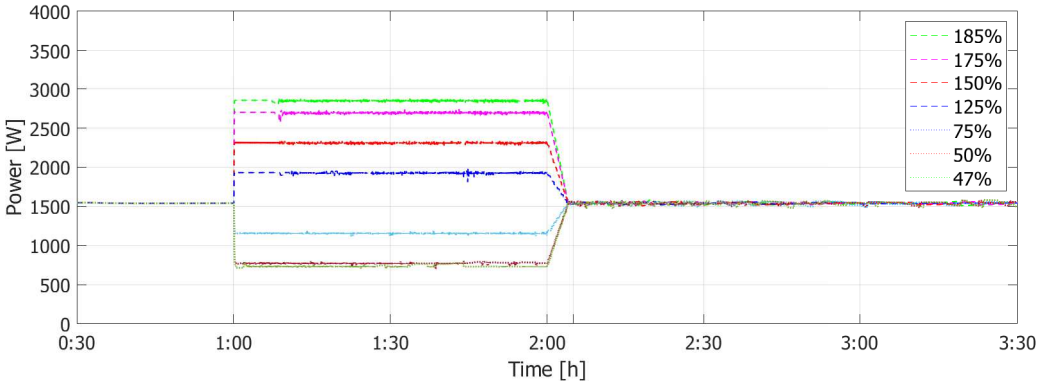

(a) Power consumed by all the TERs.

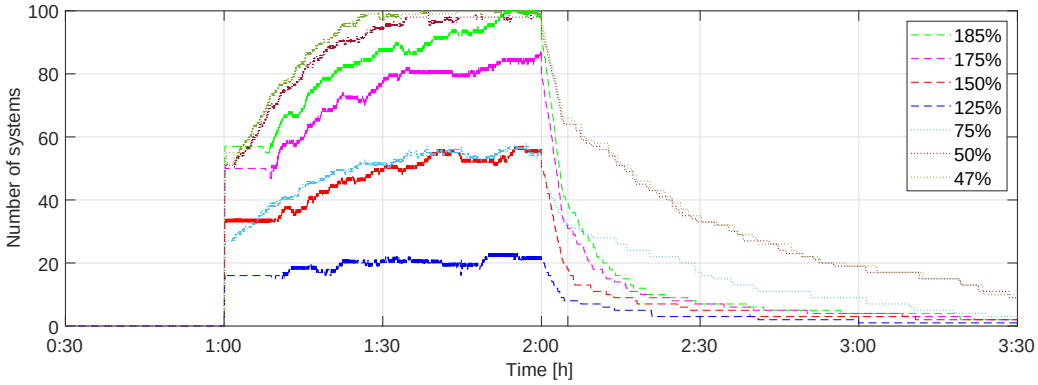

(b) Number of TERs changing the set-points.

Figure 18: Aggregator response for the Replacement Reserve (RR) service.

4. Conclusions and future work

In this work it has been shown that a set of ThermoElectric Refrigerators can be deployed to offer balancing services such as frequency containment reserve, frequency restoration re-

serve or replacement reserve by exploiting their capacity to behave as flexible loads when the temperature set-point is properly manipulated.

A dynamic model of a TER unit has been estimated from experimental data. The model root mean square error is less than 1°C and it allows to evaluate the behaviour of temperature and energy consumption under different control strategies and the response to disturbances such as introducing loads to the refrigerator or changing ambient temperature.

An aggregator to synchronise a set of TERs has been proposed. It is able to offer frequency containment reserve, frequency restoration reserve and replacement reserve services by reducing and increasing the power of some TERs. Based on a three-state signal (0, 1, or -1), the aggregator decides the temperature set-point of each TER with the aim of following the signal sent by the system operator. A modified PID controller strategy is proposed achieving a longer time interval when the TER power is zero or maximum after a set-point change, improving the offered services.

The proposed aggregator can follow a requested power trajectory in less than 30 s, arriving at 50% of the request in less than 15 s. Moreover, the information exchange between each TER and the aggregator is reduced to i) a three-state signal, ii) the power demand, and iii) the binary flexibility state. This is desirable in a fast ancillary service scheme as frequency containment reserve service, due to simplified communication requirement.

By knowing the upward and downward capacity (which depend on the current and predicted usage of the TERs in the aggregation and on the temperature preferences) and the aggregated TER baseline, the quantity offered can be established. However, the determination of the offers implies to establish not only the quantity, but also the price. These aspects, together with additional experimental evaluations considering spatially distributed TERs, will be addressed in future works. The potential use of aggregated TERs for further services (by assessing the timing constraints for providing these services, as well as the proper controller to allow the fulfilment of the network requirements) will also be studied.

Acknowledgements

Cesar Diaz-Londono received a doctoral scholarship from Program "*Rodolfo Llinás para la promoción de la formación avanzada y el espíritu científico en Bogotá*" from *Secretaría de Desarrollo Económico de Bogotá and Fundación CEIBA*.

References

[1] EurObserv'ER, "Share of renewable energy in the generation of electricity in the European Union (EU-28) from 2012 to 2017," 2019.

[2] European Commission, "Share of gross electricity generation in the European Union (EU-28) from 2016, by renewable," 2018.

[3] J. Ponocko and J. V. Milanovic, "The Effect of Load-follow-generation Motivated DSM Programme on Losses and Loadability of a Distribution Network with Renewable Generation," in *2019 IEEE PES GTD Grand International Conference and Exposition Asia (GTD Asia 2019)*, (Bangkok, Thailand), pp. 165–170, IEEE, 2019.

[4] M. Badami, G. Fambri, S. Mancò, M. Martino, I. G. Damousis, D. Agtzidis, and D. Tzovaras, "A decision support system tool to manage the flexibility in renewable energy-based power systems," *Energies*, vol. 13, no. 1, 2020.

[5] Directorate-General for Energy, "Clean energy for all Europeans," 2019.

[6] J. Chen, F. N. Lee, A. M. Breipohl, and R. Adapa, "Scheduling direct load control to minimize system operational cost," *IEEE Transactions on Power Systems*, vol. 10, no. 4, pp. 1994–2001, 1995.

[7] C. Diaz, F. Ruiz, and D. Patino, "Modeling and control of water booster pressure systems as flexible loads for demand response," *Applied Energy*, vol. 204, pp. 106–116, 2017.

[8] J. Vuelvas, F. Ruiz, and G. Gruosso, "Limiting gaming opportunities on incentive-based demand response programs," *Applied Energy*, vol. 225, no. May, pp. 668–681, 2018.

[9] M. Hosseini Imani, S. Zalzar, A. Mosavi, and S. Shamshirband, "Strategic Behavior of Retailers for Risk Reduction and Profit Increment via Distributed Generators and Demand Response Programs," *Energies*, vol. 11, no. 6, 2018.

[10] G. Chicco and A. Mazza, "New insights for setting up contractual options for demand side flexibility," *Journal of Engineering Sciences and Innovation*, vol. 4, no. 4, pp. 381–398, 2019.

[11] K. T. Ponds, A. Arefi, A. Sayigh, and G. Ledwich, "Aggregator of Demand Response for Renewable Integration and Customer Engagement: Strengths, Weaknesses, Opportunities, and Threats," *Energies*, vol. 11, no. 9, pp. 1 – 20, 2018.

[12] European Smart Grids Task Force Expert Group 3, "Demand Side Flexibility - Perceived barriers and proposed recommendations," tech. rep., 2019.

[13] B. Parrish, R. Gross, and P. Heptonstall, "On demand: Can demand response live up to expectations in managing electricity systems?," *Energy Research and Social Science*, vol. 51, pp. 107–118, 2019.

[14] F. Abbaspourtorbati, A. J. Conejo, W. Jianhui, and R. Cherkaoui, "Is Being Flexible Advantageous for Demands?," *IEEE Transactions on Power Systems*, vol. 32, no. 3, pp. 2337–2345, 2017.

[15] W. Jung and F. Jazizadeh, "Human-in-the-loop HVAC operations: A quantitative review on occupancy, comfort, and energy-efficiency dimensions," *Applied Energy*, vol. 239, no. March, pp. 1471–1508, 2019.

[16] D. Angeli and P. A. Kountouriotis, "A stochastic approach to "dynamic-demand" refrigerator control," *IEEE Transactions on Control Systems Technology*, vol. 20, no. 3, pp. 581–592, 2012.

[17] S. H. Tindemans, V. Trovato, and G. Strbac, "Decentralized Control of Thermostatic Loads for Flexible Demand Response," *IEEE Transactions on Control Systems Technology*, vol. 23, no. 5, pp. 1685–1700, 2015.

[18] R. Yin, E. C. Kara, Y. Li, N. DeForest, K. Wang, T. Yong, and M. Stadler, "Quantifying flexibility of commercial and residential loads for demand response using setpoint changes," *Applied Energy*, vol. 177, pp. 149–164, 2016.

[19] H. Hao, B. M. Sanandaji, K. Poolla, and T. L. Vincent, "Aggregate flexibility of thermostatically controlled loads," *IEEE Transactions on Power Systems*, vol. 30, no. 1, pp. 189–198, 2015.

[20] E. Kremers, J. M. González de Durana, and O. Barambones, "Emergent synchronisation properties of a refrigerator demand side management system," *Applied Energy*, vol. 101, pp. 709–717, 2013.

[21] UCTE, "A1 - Appendix 1 : Load-Frequency Control and Performance [E]," tech. rep., 204.

[22] V. Lakshmanan, M. Marinelli, A. M. Kosek, P. B. Nørgård, and H. W. Bindner, "Impact of thermostatically controlled loads' demand response activation on aggregated power: A field experiment," *Energy*, vol. 94, pp. 705–714, 2016.

[23] M. Shad, A. Momeni, R. Errouissi, C. P. Diduch, M. E. Kaye, and Liuchen Chang, "Identification and Estimation for Electric Water Heaters in Direct Load Control Programs," *IEEE Transactions on Smart Grid*, vol. 8, no. 2, pp. 947–955, 2017.

[24] E. Bompard, E. Carpaneto, G. Chicco, and R. Napoli, "Analysis and modelling of thermostatically-controlled loads," in *Proceedings of the Mediterranean Electrotechnical Conference - MELECON*, vol. 2, pp. 730–734, 1996.

[25] W. Cui, Y. Ding, H. Hui, Z. Lin, P. Du, Y. Song, and C. Shao, "Evaluation and sequential dispatch of operating reserve provided by air conditioners considering lead-lag rebound effect," *IEEE Transactions on Power Systems*, vol. 33, no. 6, pp. 6935–6950, 2018.

[26] Y. Zhou, C. Wang, J. Wu, J. Wang, M. Cheng, and G. Li, "Optimal scheduling of aggregated thermostatically controlled loads with renewable generation in the intraday electricity market," *Applied Energy*, vol. 188, pp. 456–465, 2017.

[27] M. Liu, Y. Shi, and X. Liu, "Distributed MPC of Aggregated Heterogeneous Thermostatically Controlled Loads in Smart Grid," *IEEE Transactions on Industrial Electronics*, vol. 63, pp. 1120–1129, feb 2016.

[28] W. Mai, S. Member, C. Y. Chung, and S. Member, "Economic MPC of Aggregating Commercial Buildings for Providing Flexible Power Reserve," *IEEE Transactions on Power Systems*, vol. 30, no. 5, pp. 2685–2694, 2015.

[29] D. M. Rowe, *Thermoelectrics handbook: Macro to nano.* CRC Press Taylor & Francis, boca raton ed., 2006.

[30] S. B. Riffat, S. A. Omer, and X. Ma, "A novel thermoelectric refrigeration system employing heat pipes and a phase change material : an experimental investigation," *Renewable Energy*, vol. 23, no. 2, pp. 313–323, 2001.

[31] D. Enescu, C. Diaz, A. Ciocia, A. Mazza, and A. Russo, "Experimental Assessment of the Temperature Control System for a Thermoelectric Refrigeration Unit," in *2018 53nd International Universities Power Engineering Conference (UPEC)*, pp. 1–6, 2018.

[32] C. Diaz-Londono, D. Enescu, A. Mazza, and F. Ruiz, "Characterization and Flexibility of a ThermoElectric Refrigeration Unit," in *2019 54th International Universities Power Engineering Conference (UPEC)*, pp. 1–6, 2019.

[33] E. Söylemez, E. Alpman, and A. Onat, "Experimental analysis of hybrid household refrigerators including thermoelectric and vapour compression cooling systems," *International Journal of Refrigeration*, vol. 95, pp. 93–107, 2018.

[34] C. J. L. Hermes and J. R. Barbosa, "Thermodynamic comparison of Peltier, Stirling, and vapor compression portable coolers," *Applied Energy*, vol. 91, no. 1, pp. 51–58, 2012.

[35] P. K. Bansal and A. Martin, "Comparative study of vapour compression, thermoelectric and absorption refrigerators," *International Journal of Energy Research*, vol. 24, no. 2, pp. 93–107, 2000.

[36] D. Zhao and G. Tan, "Experimental evaluation of a prototype thermoelectric system integrated with PCM (phase change material) for space cooling," *Energy*, vol. 68, pp. 658–666, 2014.

[37] J. S. Lewis, I. Chaer, and S. A. Tassou, "Reviews of Alternative Refrigeration Technologies," Tech. Rep. July, School of Engineering and Design, 2007.

[38] D. Enescu, A. Ciocia, A. Mazza, and A. Russo, "Solutions based on thermoelectric refrigerators in humanitarian contexts," *Sustainable Energy Technologies and Assessments*, vol. 22, pp. 134–149, 2017.

[39] D. Zhao and G. Tan, "A review of thermoelectric cooling: Materials, modeling and applications," *Applied Thermal Engineering*, vol. 66, no. 1-2, pp. 15–24, 2014.

[40] R. Opoku, S. Anane, I. A. Edwin, M. S. Adaramola, and R. Seidu, "Comparative techno-economic assessment of a converted DC refrigerator and a conventional AC refrigerator both powered by solar PV," *International Journal of Refrigeration*, vol. 72, pp. 1–11, 2016.

[41] D. Astrain, P. Aranguren, A. Martínez, A. Rodríguez, and M. G. Pérez, "A comparative study of different heat exchange systems in a thermoelectric refrigerator and their influence on the efficiency," *Applied Thermal Engineering*, vol. 103, pp. 1289–1298, 2016.

[42] A. Martínez, D. Astrain, and A. Rodríguez, "Dynamic model for simulation of thermoelectric self cooling applications," *Energy*, vol. 55, pp. 1114–1126, 2013.

[43] D. Astrain, A. Martínez, and A. Rodríguez, "Improvement of a thermoelectric and vapour compression hybrid refrigerator," *Applied Thermal Engineering*, vol. 39, pp. 140–150, 2012.

[44] R. R. He, H. Y. Zhong, Y. Cai, D. Liu, and F. Y. Zhao, "Theoretical and Experimental Investigations of Thermoelectric Refrigeration Box Used for Medical Service," *Procedia Engineering*, vol. 205, pp. 1215–1222, 2017.

[45] S. Jugsujinda, A. Vora-Ud, and T. Seetawan, "Analyzing of thermoelectric refrigerator performance," in *2nd International Science, Social-Science, Engineering and Energy Conference 2010: Engineering Science and Management*, vol. 8, pp. 154–159, 2011.

[46] D. Astrain, A. Martínez, J. Gorraiz, A. Rodríguez, and G. Pérez, "Computational Study on Temperature Control Systems for Thermoelectric Refrigerators," *Journal of Electronic Materials*, vol. 41, no. 6, pp. 1081–1090, 2012.

[47] A. Martínez, D. Astrain, A. Rodríguez, and G. Pérez, "Reduction in the electric power consumption of a thermoelectric refrigerator by experimental optimization of the temperature controller," *Journal of Electronic Materials*, vol. 42, no. 7, pp. 1499–1503, 2013.

[48] The European Commission, "Commission Regulation (EU) 2017/2195 of 23 November 2017 establishing a guideline on electricity balancing.," *Official Journal of the European Union*, vol. 2017, no. November, pp. 312/6 – 312/53, 2017.

[49] Y. V. Makarov, C. Loutan, J. Ma, and P. de Mello, "Operational impacts of wind generation on California power systems," *IEEE Transactions on Power Systems*, vol. 24, no. 2, pp. 1039–1050, 2009.

[50] A. Ulbig and G. Andersson, "Analyzing operational flexibility of electric power systems," *International Journal of Electrical Power and Energy Systems*, vol. 72, pp. 155–164, 2015.

[51] European Commission, "Commission Regulation (EU) 2017/1485 establishing a guideline on electricity transmission system operation," *Official Journal of the European Union*, vol. L 220, pp. 1–120, 2017.

[52] ENTSO-E, "All TSOs' proposal for the implementation framework for a European platform for the exchange of balancing energy from frequency restoration reserves with manual activation in accordance with Article 20 of Commission Regulation (EU) 2017/2195 establishing a guideline on electricity balancing," tech. rep., 2018. https://consultations.entsoe.eu/markets/mfrr˙implementation˙framework.

[53] ENTSO-E, "All TSOs' proposal for the implementation framework for the exchange of balancing energy from frequency restoration reserves with automatic activation in accordance with Article 21 of Commission Regulation (EU) 2017/2195 establishing a guideline on electricity balancing," tech. rep., 2018. https://consultations.entsoe.eu/markets/afrr˙implementation˙framework.

[54] ENTSO-E, "The proposal of all TSO performing the reserve replacement process for the implementation framework for the exchange of balancing energy from Replacement Reserves in accordance with Article 19 of Commission Regulation (EU) 2017/2195 of 23 November 2017 establishing a guideline on electricity balancing,"

tech. rep., 2018. https://consultations.entsoe.eu/markets/implementation-framework-replacement-reserves.

[55] G. Min and D. M. Rowe, "Experimental evaluation of prototype thermoelectric domestic-refrigerators," *Applied Energy*, vol. 83, no. 2, pp. 133–152, 2006.

[56] R. Saidur, H. H. Masjuki, M. Hasanuzzaman, T. M. I. Mahlia, C. Y. Tan, J. K. Ooi, and P. H. Yoon, "Performance investigation of a solar powered thermoelectric refrigerator," *International Journal of Mechanical and Materials Engineering*, vol. 3, no. 1, pp. 7–16, 2008.

[57] The European Parliament and the Council of the European Union, "Regulation (EC) No 852/2004 of the European Parliament and of the Council of 29 April 2004 on the hygiene of foodstuffs," *Official Journal of the European Union*, no. L 139/1, pp. 1–54, 2004.

[58] Food Standards Agency (FSA), "Guidance on Temperature Control Legislation in the United Kingdom," pp. 1–17, 2016.

[59] Food Standards Australia New Zealand (FSANZ), "Essential food safety practices. Cool and reheat food safely to the right temperatures," 2017.